Picosecond solvation dynamics of alkali cations in superfluid ^{4}He nanodroplets

Antonio Leal,[1] David Mateo,[1,2] Alberto Hernando,[3] Martí Pi,[1] Manuel Barranco,[1] Alessandro Ponti,[4] Fausto Cargnoni,[4] and Marcel Drabbels[5]

[1]*Departament ECM, Facultat de Física, and IN^{2}UB, Universitat de Barcelona, Diagonal 645, 08028 Barcelona, Spain*

[2]*Department of Chemistry and Biochemistry, California State University at Northridge, 18111 Nordhoff St., Northridge, California 91330, USA*

[3]*Laboratory of Theoretical Physical Chemistry, Institut des Sciences et Ingénierie Chimiques, Swiss Federal Institute of Technology Lausanne (EPFL), CH-1015 Lausanne, Switzerland*

[4]*Istituto di Scienze e Tecnologie Molecolari (ISTM), Consiglio Nazionale delle Ricerche, via Golgi 19, 20133 Milano, Italy*

[5]*Laboratoire de Chimie Physique Moléculaire, Swiss Federal Institute of Technology Lausanne (EPFL), CH-1015 Lausanne, Switzerland*

(Received 10 September 2014; revised manuscript received 29 October 2014; published 19 December 2014)

The dynamics following the photoionization of neutral Rb and Cs atoms residing in a dimple at the surface of a superfluid $^4He_{1000}$ nanodroplet has been investigated within time-dependent density functional theory, complementing a previous study on Ba. The calculations reveal that structured high density helium solvation layers form around both the Rb^+ and Cs^+ cation on a picosecond time scale, forming so-called snowballs. In contrast to the Rb^+ ion, Cs^+ is not solvated by the $^4He_{1000}$ droplet but rather desorbs from it as a Cs^+He_n snowball. This outcome is partially related to the large size of Cs^+ cation in relation to the helium droplet as is revealed by calculations performed using a planar helium surface. The large droplet deformations induced by the solvation of the Rb^+ cation is found to lead to efficient nucleation of quantized vortex loops or rings.

DOI: 10.1103/PhysRevB.90.224518 PACS number(s): 36.40.Wa, 32.30.Jc, 67.25.dw, 67.25.dk

I. INTRODUCTION

Ions are often used as probes to investigate the properties of superfluid liquid helium by determining their mobility (see Refs. [1–4], and references therein). Due to electrostriction, the positive ion locally perturbs the superfluid so strongly that in most cases it is surrounded by very inhomogeneous, high density helium solvation layers [2]. The solvation structure, which depends strongly on the ionic species, is a nanoscopic solidlike complex that rigidly moves along with the cation, hence its name "snowball" [5]. Potentially these ionic snowballs can also be used to probe the properties of helium nanodroplets. These droplets are created by condensation of the expanding helium gas and reach a limiting temperature of about 0.37 K [6,7], clearly below the superfluid transition temperature in liquid ^{4}He, $T_\lambda = 2.17$ K. Early Quantum Monte Carlo (QMC) calculations indicated that a very small droplet containing less than 100 atoms already displays features pertaining to the superfluid state of bulk liquid helium [8–11]. This was later confirmed in a cornerstone experiment by Toennies and co-workers on mixed ^{3}He-^{4}He droplets doped with carbonyl sulfide (OCS) [12]. The solvated OCS molecule was found to display a rotationally resolved vibrational spectrum, indicating that it rotates inside the ^{4}He core of the mixed droplet. The minimum number of ^{4}He atoms in the core needed to produce the effect was found to be about 60, in good agreement with the calculations [8].

Another manifestation of superfluidity is the frictionless displacement of impurities inside helium if they move at velocities below the so-called critical Landau velocity v_L. This property is due to the peculiar maxon-roton structure of the superfluid excitation spectrum. Impurities moving inside a superfluid helium droplet would lose their translational energy by exciting elementary excitation until reaching a velocity below v_L. Consequently, if impurities are ejected from the droplet their velocity distribution should display a limiting velocity. This has been recently established for several atomic and molecular impurities in droplets consisting of just 1000 helium atoms [13,14].

The appearance of quantized vortices is yet another manifestation of superfluidity. First experimental indications of the presence of vortices in helium droplets was provided by the surface deposition of large droplets doped with Ag atoms [15]. Upon impact, the helium atoms evaporate while the Ag atoms remain on the surface keeping their "*in situ*" cluster structure, revealing a filamentlike distribution corresponding to the vortex line they were originally attached to inside the droplet. Experiments for other atomic impurities have been recently conducted, where the presence of vortex lines in helium droplets has been exploited to guide the formation of ultrathin nanowires [16–18].

Very recently, in a femtosecond x-ray coherent diffractive imaging experiment the existence of vortex arrays in helium droplets has been confirmed [19]. The diffraction images revealed characteristic Bragg patterns from Xe clusters trapped on the vortex cores present in the helium droplets. These droplets are produced by fragmentation of a cryogenic fluid and consist of $N = 10^8$–10^{11} atoms and are thus true mesoscopic pieces of superfluid helium. Hence, it is not surprising that they host vortex lines, which either preexist in the expanding fluid or are created in the fragmentation process.

A different question is whether vortices nucleate when droplets are created by condensation of an expanding gas which is the method used to produce helium droplets containing several thousand atoms [20]. In principle, these droplets can carry enough energy and angular momentum to create a vortex. Moreover, in experiments with doped droplets the pickup process might lead to vortex nucleation. Once nucleated, pinning to the impurity would stabilize a vortex inside the droplet due to the lack of decay channels that conserve both energy and angular momentum [21,22]. The experimental detection of vortices in helium droplets made of

a few thousand He atoms is, however, a still unsolved issue. It is expected that they could be detected by spectroscopic techniques [23,24] as their presence affects the spectrum of the dopants they contain [25,26]. However, for the systems considered the width of the absorption spectrum is larger than the shift introduced by the presence of the vortex, thereby impeding the possible detection of vortices [27,28].

Ionization of an impurity in a helium droplet leads to a strong perturbation of the system since the created cation interacts more strongly with the helium than its neutral precursor. For an impurity residing at the surface of a helium droplet, such as an alkali atom or heavy alkaline-earth atom, the cation is expected to become fully solvated by the helium, i.e., sink into the helium droplet. Several studies indeed indicate that following the ionization of alkali atoms the created cations remain attached to the droplet [29–32]. These experiments, however, provide no details on the location of the cation. Recently the complete solvation of a cation has been experimentally confirmed for Ba^+. The $6p\ ^2P \leftarrow 6s\ ^2S$ absorption spectrum of the Ba^+ cation was found to be identical to that obtained in bulk liquid He, indicating that the ion becomes indeed solvated by the droplet within the 100 ns time scale of the experiment [33]. The solvation dynamics of the Ba^+ has also been addressed theoretically within time-dependent density functional theory (TDDFT) for the $Ba@He_{1000}$ system [28]. It was found that due to the relatively strong ion-helium interaction, the velocity of the Ba^+ cation during the solvation process temporarily exceeds v_L, leading to the nucleation of a quantized ring vortex. The calculated $6p\ ^2P \leftarrow 6s\ ^2S$ absorption spectrum of Ba^+ revealed a clear time dependence due to the solvation of the ion but was not noticeably affected by the presence of the ring vortex [28].

Here we report TDDFT calculations on the solvation dynamics of Rb^+ and Cs^+ cations produced by ionization of the neutral precursor initially located at the surface of a $^4He_{1000}$ droplet. The work on these systems is motivated by recent experiments which reveal that upon ionization extended snowball distributions up to $Rb^+@^4He_{41}$ and $Cs^+@^4He_{41}$ are formed [34], showing distinct intensity steps at masses corresponding to $Rb^+@^4He_{14}$ and $Cs^+@^4He_{16}$. These steps have been identified as the filling of the first solvation shell around the cation, somewhat defining the snowball. In addition, these two systems complement our work on Ba^+ [28]. Since compared to Ba^+, the interaction of an alkali cation with helium is much stronger, the results will provide additional insight into the snowball formation and the nucleation of vortices in small helium droplets.

II. THEORETICAL APPROACH

A. He-dopant pair potentials

One of the key ingredients for the simulations presented in this study are the potential energy curves (PEC) between helium atoms and neutral or charged dopants. The Rb-He and Cs-He ground state pair potentials have been taken from Ref. [35]. These potentials are based on perturbative calculations but agree well with recent *ab initio* computations for Rb-He [36–38] and Cs-He [38] carried out at the CCSD(T) level of theory adopting extended basis sets.

For Rb^+ and Cs^+ cations, the available potentials date back to 1990 [39], and have been essentially obtained by inversion of experimental data. To determine them we performed computations at the CCSD(T) level of theory, as implemented in the MOLPRO 2010 computational code [40]. The core electrons of the metal atoms have been described with the dhf pseudopotential [41], and for the valence electrons we selected the QZVP Gaussians basis set [42]. The aug-cc-pV5Z basis [43] has been adopted for helium, and a $3s3p2d$ set of bond functions [44] has been placed midway between the two nuclei. The interaction energy has been determined in the range from 2 to 12 Å at 33 (38) internuclear distances in the case of Rb^+-He (Cs^+-He), using the standard counterpoise technique proposed by Boys and Bernardi [45]. The spatial grids finely sample (i.e., with 0.1 Å steps) the regions of the repulsive wall and the attractive well of the potentials, while sparser grids are selected for the long-range tail. We also conducted test computations on Rb^+-He at the CCSD(T) level of theory, either adopting the Def2 pseudopotential [46] on the metal atom, and the larger QZVPP basis set [42]. The changes in the computed interaction energy are very small, and do not play a relevant role in the simulation of the dynamics of $Rb^+@^4He_N$ aggregates.

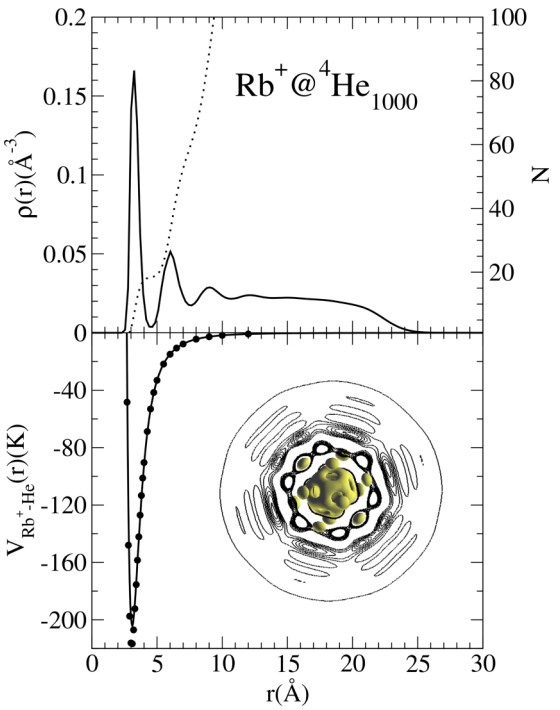

FIG. 1. (Color online) Top panel: Solid line, spherically averaged helium density profile of the $Rb^+@^4He_{1000}$ complex, left scale. Dotted line, number of ^4He atoms as a function of distance to the cation, right scale. Bottom panel: Solid line, Rb^+-He pair potential of Ref. [39]; dots, pair potential calculated in this work. Next to them, the nonaveraged helium density around the cation is shown by means of surfaces of constant density $\rho = 0.08$ Å^{-3}. Ten isodensity contours in a plane passing through the center of the complex are shown in the 0.04–0.0218 Å^{-3} range.

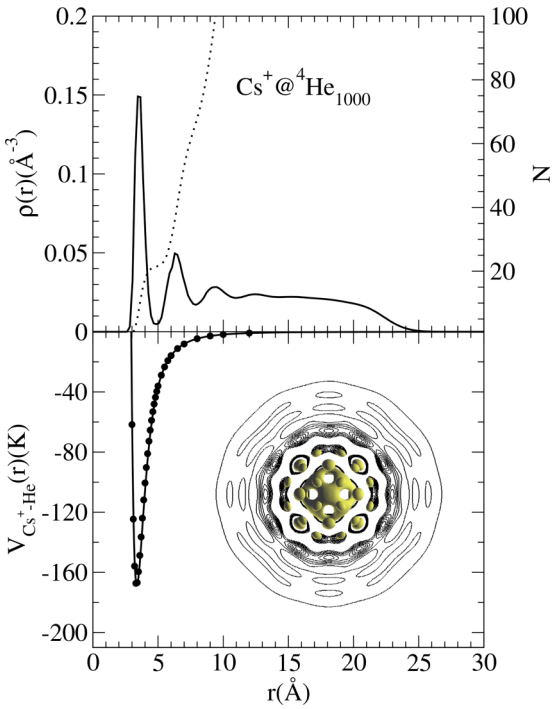

FIG. 2. (Color online) Top panel: Solid line, spherically averaged helium density profile of the $Cs^+@^4He_{1000}$ complex, left scale. Dotted line, number of ^{4}He atoms as a function of distance to the cation, right scale. Bottom panel: Solid line, Cs^+-He pair potential of Ref. [39]; dots, pair potential calculated in this work. Next to them, the nonaveraged helium density around the cation is shown by means of surfaces of constant density $\rho = 0.08$ Å^{-3}. Ten isodensity contours in a plane passing through the center of the complex are shown in the 0.04–0.0218 Å^{-3} range.

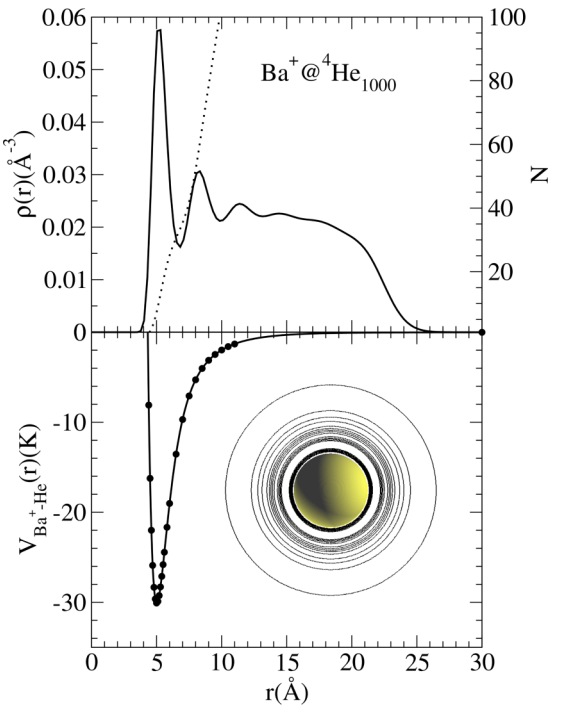

FIG. 3. (Color online) Top panel: Solid line, helium density profile of the $Ba^+@^4He_{1000}$ complex, left scale. Dotted line, number of ^{4}He atoms as a function of distance to the cation, right scale. Bottom panel: Dots, Ba^+-He pair potential [28]. Solid line, fit to the pair potential used in this work that includes a r^{-4} term appropriate for cation-atom potentials. Next to it, the helium density around the cation is shown by means of a surface of density $\rho = 0.05$ Å^{-3}. Ten isodensity contours in a plane passing through the center of the complex are shown in the 0.04–0.0218 Å^{-3} range.

Figures 1 and 2 show the CCSD(T) pair potentials, whose features are consistent with the ionic radii of the two cations: As one moves from Rb^+ to Cs^+ (i.e., increases the size of the charged species) the potential well shifts to larger internuclear distances and its depth decreases. Interestingly, in the two PEC the internuclear distance at the minimum potential energy is quite close to the sum of the ionic radius of the cation and the van der Waals radius of helium (3.06 and 3.21 Å for Rb^+-He and Cs^+-He, respectively). This suggests that in both systems electronic repulsion takes place as soon as the electronic clouds of the cation and helium overlap.

As can be seen in Fig. 2, in the case of Cs^+-He there are no significant differences between our PEC and that proposed by Koutselos *et al.* [39]. We obtain a minimum interaction energy of −169 K at the internuclear distance of 3.35 Å, to be compared with their value of −169 K at 3.47 Å. In the case of Rb^+-He the gross features of both potentials are also similar, but the attractive well calculated at the CCSD(T) level (−218 K) is 5% deeper (−204 K) [39]. The internuclear distance at the minimum is 3.05 Å for both potentials. For this reason, we carried out simulations using both PECs in the case of Rb^+. The results turned out to be very similar and consequently in the following we only discuss those obtained with the CCSD(T) potential. For completeness, we also show in Fig. 3 the He-Ba^+ pair potential [28]. The potential is much less attractive (−30.1 K) as compared to the Rb^+-He and Cs^+-He potentials, and the attractive well is located at larger internuclear distances (5.0 Å) due to the presence of an electron in the 6*s* orbital of barium.

B. DFT for bosons

We address the static and dynamic properties of doped helium droplets within density functional theory (DFT) [47]. In its static version, this approach has been successfully applied to the study of many problems in bulk liquid helium and droplets (see Ref. [48], and references therein). The development of TDDFT methods applicable to microscopic superfluids [49,50] has opened the way to a real-time description of doped droplets in a size range of experimental interest [14,28,51]. Besides DFT, we have used the Born-Oppenheimer approximation to factorize the electronic and nuclear wave functions, the Franck-Condon approximation which assumes that the atomic nuclei do not change their positions or momenta during the electronic transition, and the diatomics-in-molecules approximation [52].

We have considered a droplet made of $N = 1000$ helium atoms and have first obtained the structure of the neutral alkali-droplet complex in the ground state. Due to the large mass of Rb and Cs atoms compared to that of He, we describe them as classical particles in the dynamics while their effect on the statics is incorporated as an external field acting upon

the droplet [14,53]. Accordingly, the energy of the system is written as

$$E[\rho] = \int d\mathbf{r} \left\{ \frac{\hbar^2}{2m_{\mathrm{He}}} |\nabla \sqrt{\rho(\mathbf{r})}|^2 + \mathcal{E}_{\mathrm{He}}[\rho(\mathbf{r})] \right\} + \int d\mathbf{r}\, \rho(\mathbf{r})\, V_X(|\mathbf{r}_{\mathrm{Ak}} - \mathbf{r}|), \quad (1)$$

where $\mathcal{E}_{\mathrm{He}}$ is the potential energy density per unit volume, Ak represents either the Rb or Cs atom, $\rho(\mathbf{r})$ is the He particle density at point $\mathbf{r}$, and $\mathbf{r}_{\mathrm{Ak}}$ is the impurity location.

As indicated, the Rb-He and Cs-He ground state pair potentials V_X have been taken from Ref. [35]. The DF used in the present work [54] is a modified version of the Orsay-Trento functional [47] able to handle very structured helium configurations as those expected to appear around fairly attractive impurities as cations. Examples of such configurations for several alkali and alkaline-earth ion snowballs obtained by static DFT calculations can be found in Refs. [4,55,28].

Upon variation of Eq. (1) one obtains the Euler-Lagrange equation that is solved to determine the equilibrium density $\rho_0(\mathbf{r})$ of the droplet and the location of the dopant atom $\mathbf{r}_{\mathrm{Ak}_0}$ [56]. Schematically,

$$\frac{\delta}{\delta\rho}\left(\frac{\hbar^2}{2m_{\mathrm{He}}} \left|\nabla\sqrt{\rho}\right|^2 + \mathcal{E}_{\mathrm{He}} \right) + V_X = \mu, \quad (2)$$

where μ is the chemical potential of the He droplet.

Equation (2) has been solved in Cartesian coordinates using a spatial grid of 0.4 Å and a 200×200×250 point mesh. The derivatives have been calculated with 13-point formulas. Extensive use of fast-Fourier techniques [57] has been made to efficiently calculate the energy density and mean field potential [14,51]. The calculations indicate that the alkali atoms are located on the surface of the droplets. A two-dimensional plot of the resulting helium dimple structure for Rb and Cs can be found in Fig. 3 of Ref. [56].

The dynamics is triggered by the sudden substitution of the Ak-He ground state pair potential V_X by that corresponding to Ak^+-He, V_X^+. Since the resulting $Ak^+@^4He_{1000}$ configuration is not at equilibrium, the system evolves in time. Within TDDFT, we represent the He droplet by a complex effective wave function $\Psi_{\mathrm{He}}(\mathbf{r},t)$ such that $\rho(\mathbf{r},t) = |\Psi_{\mathrm{He}}(\mathbf{r},t)|^2$. The position of the Ak^+ cation $\mathbf{r}_{Ak^+}(t)$ obeys the Newton equation. Consequently,

$$\begin{aligned} i\hbar\frac{\partial}{\partial t}\Psi_{\mathrm{He}} &= \left[-\frac{\hbar^2}{2m_{\mathrm{He}}}\nabla^2 + \frac{\delta\mathcal{E}_{\mathrm{He}}}{\delta\rho(\mathbf{r})} + V_X^+(|\mathbf{r} - \mathbf{r}_{Ak^+}|) \right]\Psi_{\mathrm{He}}, \\ m_{Ak^+}\ddot{\mathbf{r}}_{Ak^+} &= -\nabla_{\mathbf{r}_{Ak^+}} \left[\int d\mathbf{r}\, \rho(\mathbf{r}) V_X^+(|\mathbf{r} - \mathbf{r}_{Ak^+}|) \right] \\ &= -\int d\mathbf{r} [\nabla\rho(\mathbf{r})] V_X^+(|\mathbf{r} - \mathbf{r}_{Ak^+}|). \end{aligned} \quad (3)$$

The initial condition to solve Eqs. (3) is the equilibrium droplet-neutral Ak configuration, $\Psi(\mathbf{r},t=0) = \sqrt{\rho_0(\mathbf{r})}$, $\mathbf{r}_{Ak^+}(t=0) = \mathbf{r}_{\mathrm{Ak}_0}$. The initial velocity of the Ak^+ cation is set to zero. Equations (3) have been solved using the same grid as for the static problem and a time step of 0.5 fs. We have used for both a predictor-corrector method fed by a few time steps obtained by a fourth-order Runge-Kutta algorithm [58].

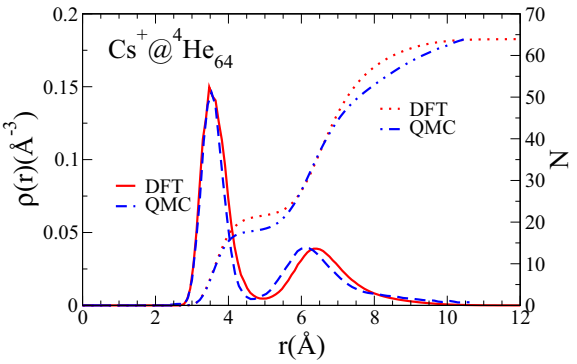

FIG. 4. (Color online) Comparison between the spherically averaged DFT density profile (solid line) and QMC density profile [3] (dashed line) for the $Cs^+@^4He_{64}$ complex, left scale. Also shown is the number of ^{4}He atoms as a function of distance to the cation, right scale.

III. RESULTS

A. Statics

It has been experimentally determined that alkali atoms reside at the surface of ^{4}He droplets [56,59], a result that is reproduced by DFT calculations [56]. At variance, Rb^+ and Cs^+ cations are fully solvated and develop snowball structures [3]. The calculated equilibrium configuration of $Rb^+@^4He_{1000}$ and $Cs^+@^4He_{1000}$ are shown in Figs. 1 and 2, respectively. In both cases, a highly structured helium density appears around the cation, in agreement with variational and QMC calculations [3,60]. The spherically averaged helium number density shown in Figs. 1 and 2 as a function of distance to the cation reveals a clear shell structure. By integrating this density over the radial coordinate the number of helium atoms in the solvation shells can be determined. Using this procedure the first solvation shell is found to host 19.2 (21.4) atoms for Rb^+ (Cs^+). These values are somewhat larger than those found experimentally [32,34] and by QMC calculations [3]. Figure 3 shows the equilibrium configuration of $Ba^+@^4He_{1000}$. In contrast to Rb^+ and Cs^+, the Ba^+ ion is found to be surrounded by a smooth and unstructured helium density, in agreement with QMC calculations [61]. This difference is a direct consequence of the much weaker interaction of the Ba^+ ion with the helium, *vide supra*.

For the sake of comparison, we show in Fig. 4 the spherically averaged DFT density profile and QMC density profile corresponding to the $Cs^+@^4He_{64}$ droplet [3]. It can be seen that the minor discrepancy mainly appears in the second solvation shell. This seems to be a very general trend [4,55], likely reflecting that the occupancy of the first solvation shell is essentially determined by the impurity-droplet interaction and is less sensitive to the theoretical approach used to describe the system.

Using these helium densities we have calculated the zero electron kinetic energy (ZEKE) spectrum for Rb, Cs, and Ba. Besides being interesting by itself [62], the ZEKE spectrum probes the structure of the surface dimple state of the dopant atom and the accuracy of the He-cation ground state pair potential. Since the impurities are described classically and the electron orbitals are not explicitly included, the ZEKE

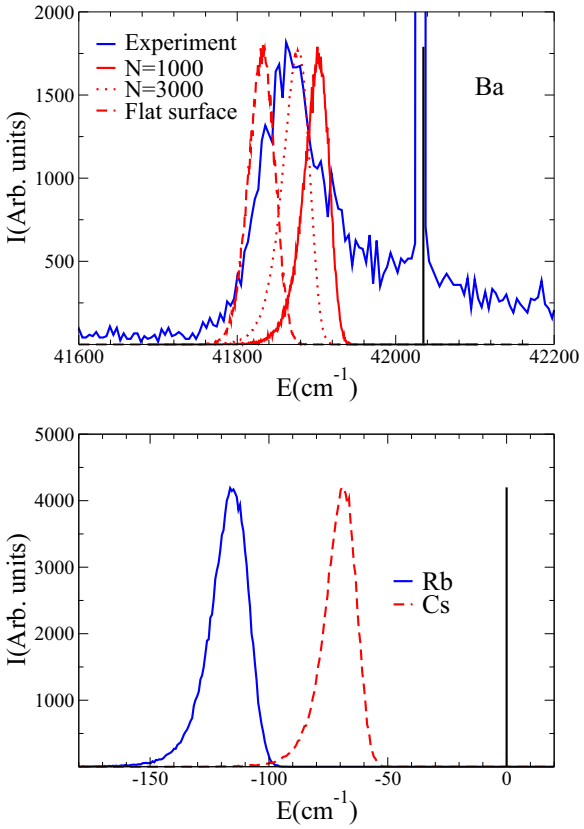

FIG. 5. (Color online) Top panel: ZEKE spectrum for Ba in arbitrary units. Dashed line, experimental result for a $N = 2700$ droplet [62]. Calculated spectra: solid line, $^4He_{1000}$ droplet; squares, $^4He_{3000}$ droplet; dotted line, helium flat surface. The ionization energy of the Ba atom is 42 034.91 cm^{-1} (vertical line) [65]. Bottom panel: Calculated ZEKE spectrum in arbitrary units for Rb (solid line) and Cs (dashed line) in a $N = 1000$ droplet. In both cases, the spectrum refers to the ionization energy (vertical line), 33 690.81 cm^{-1} for Rb and 31 406.47 cm^{-1} for Cs, respectively [65].

spectrum is calculated from the semiclassical approximation of the vibrational Franck-Condon factors of an instantaneous transition from the neutral ground state to the ionic state. This is written as the vertical transition of the atom from the ground state well potential to that of the Ak^+-He well for the same helium configuration:

$$\Delta\omega = \int d\mathbf{r}\, \rho_0(\mathbf{r})\, [V_X^+(|\mathbf{r}_{Ak_0} - \mathbf{r}|) - V_X(|\mathbf{r}_{Ak_0} - \mathbf{r}|)]. \quad (4)$$

The above expression gives the peak position for a given configuration referenced to the ionization energy of a free atom. The complete spectrum is obtained by DF sampling of the helium density [63].

For the case of barium, the Ba-He and Ba^+-He pair potentials have been taken from Refs. [64,28], respectively. The ZEKE spectrum of $Ba^+@^4He_{1000}$, referenced to the ionization energy of Ba, 42 034.91 cm^{-1} [65], is shown in Fig. 5. The experimental spectrum corresponding to a $\bar{N} = 2700$ droplet [62], which is also shown in this figure, has a long tail towards high energies. This tail has been attributed to the presence of autoionizing states in the continuum and consequently should not be considered when comparing to the calculations. The calculated ZEKE spectrum for the $N = 1000$ droplet clearly reveals a smaller shift from the atomic ionization threshold than the experimental spectrum. This apparent disagreement between theory and experiment is likely a finite-size (curvature) effect [66]. To confirm this conjecture we have calculated ZEKE spectra for a $N = 3000$ droplet and also for a flat helium surface (see Sec. III B). The corresponding results which are shown in the top panel of the figure reveal a much better agreement with experiment.

The ZEKE spectra of Rb and Cs presented in Fig. 5 have been calculated using the Ak-He pair potentials available in the literature [35] and the ionic potentials calculated in present work. For these two species, no experimental information is available. A comparison reveals that the helium induced shift is significantly larger for Rb than for Cs. This can be attributed to a stronger Rb^+-He interaction (see Figs. 1 and 2) and the deeper dimple structure for Rb compared to Cs [56]. The calculated shifts are significantly larger than the ionization thresholds that have been determined by extrapolation of the Rydberg series for these systems [67,68], or measured directly via two-step ionization [31]. This difference can be attributed to the fact that experiment and theory do not probe the same ionization threshold. In our calculations we determine the ionization threshold for the direct ionization of the system. In the aforementioned experiments the system is first excited to an intermediate state from which the higher excited states are probed. Following excitation to this intermediate state the system relaxes as the helium rearranges around the excited atom. Consequently, in the experiments the ionization threshold is measured not for the ground state helium configuration but rather for that corresponding to an excited atom. This is thought to be the main reason for the difference between the experimental and theoretical results. This assumption is supported by the ZEKE spectra recorded for ground state and excited Ba atoms on helium droplets [62]. Here the reduction of the ionization threshold for the excited atom was about half of that found for the ground state configuration. A similar difference in the ionization shift is seen here for the Rb and Cs atoms when comparing the experimental and theoretical data. In addition, the calculated shifts match very well the experimentally observed shift for ground state Na atoms on helium droplets [30,69]. In view of this we conclude that the initial position of the impurities as well as their interaction with the helium are accurately described in the present calculations.

B. Dynamics

The static calculations have shown that the equilibrium configuration of the cation-droplet system corresponds to a fully solvated impurity residing in the bulk of the droplet. Based on our work on Ba, it is expected that upon creation of an alkali cation at the surface of a helium droplet the ion becomes fully solvated on a time scale on the order of 10 ps [28]. Figure 6 shows snapshots of the dynamical evolution of the $Rb^+@^4He_{1000}$ system. Inspection of the multimedia material [70], as well as integration of the helium density inside the first solvation shell around the impurity as a function of time, reveals that a snowball structure fully develops in about 20 ps. Notice that the formation of the snowball breaks the axial

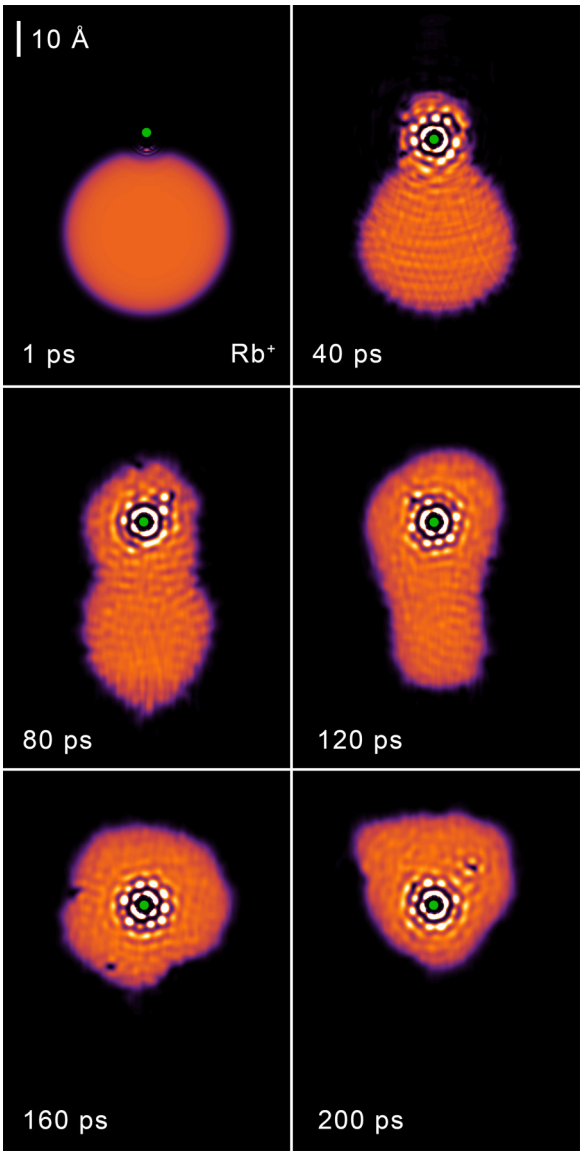

FIG. 6. (Color online) Dynamic evolution of the $Rb^+@^4He_{1000}$ complex when the neutral Rb is suddenly ionized. The corresponding time is indicated in each frame. The dark spots in the $t = 160$ and 200 ps frames are the cross section of nucleated vortex loops (see Fig. 12).

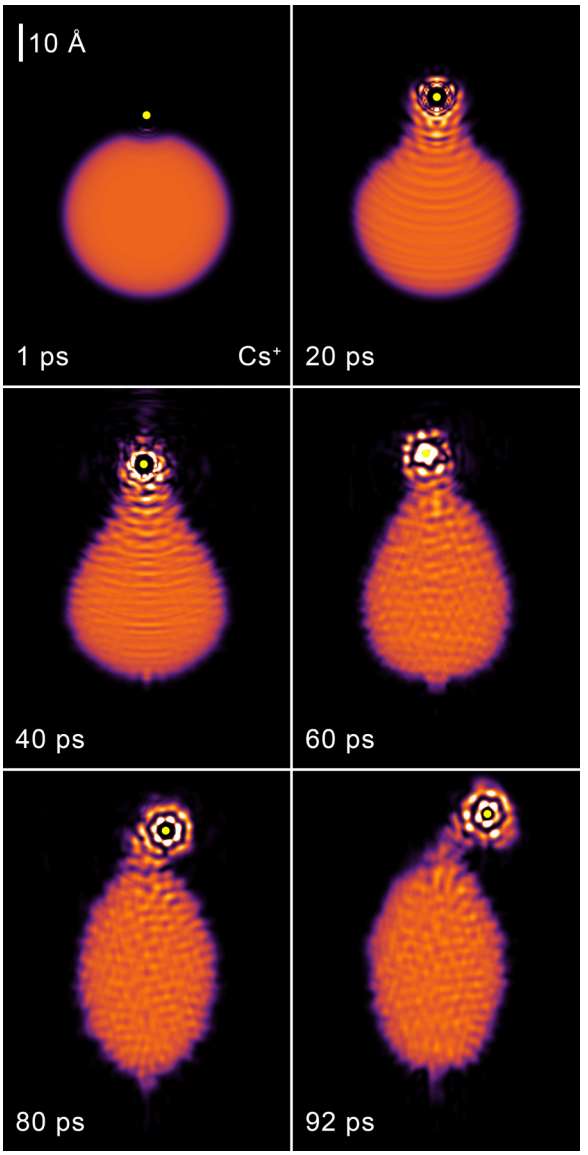

FIG. 7. (Color online) Dynamic evolution of the $Cs^+@^4He_{1000}$ complex when the neutral Cs is suddenly ionized. The corresponding time is indicated in each frame.

symmetry of the system, much like density fluctuations tend to do. This strongly affects the subsequent dynamics of the snowball structure and leads to a loss of the axial symmetry of the droplet. After the formation of the Rb^+ snowball, the whole structure becomes solvated by helium on a 100 ps time scale. During the entire dynamics the Rb^+ ion remains almost stationary while the helium rearranges around the ion. We have found the same behavior and time scales when using the He-Rb^+ pair potential of Ref. [39], even though this interaction potential is less attractive than the one we have calculated here. If one compares the result for Rb^+ with the dynamics of the Ba^+ cation whose interaction with the helium is much weaker [28], one finds noticeable differences between the way these ions become solvated. Whereas the Rb^+ ion remains almost stationary as the helium rearranges, the Ba^+ was found to sink into the helium droplet and to perform a nearly undamped oscillatory motion inside the droplet. The initial position of the cation, i.e., the depth of the dimple structure, as well as the interaction strength thus clearly have a strong effect on the dynamical evolution of the system.

Since the Cs^+-He and Rb^+-He interaction potentials as well as the initial helium dimple structures are quite similar, at least when compared to barium, one expects very similar dynamics for these two alkali ions. Inspection of Fig. 7, which shows the dynamical evolution of the $Cs^+@^4He_{1000}$ system, reveals that like for Rb^+ a solvation shell develops around the Cs^+. The time scale of 30 ps is somewhat longer than for Rb^+, which can be attributed to the slightly weaker interaction of the Cs^+ with the helium and the larger distance between the cation and the droplet. Quite unexpectedly, we find that the Cs^+ cation does not become fully solvated by the helium. Rather it desorbs from the droplet as a snowball containing about 75 helium atoms after $t \gtrsim 90$ ps (see Fig. 8). Thus although

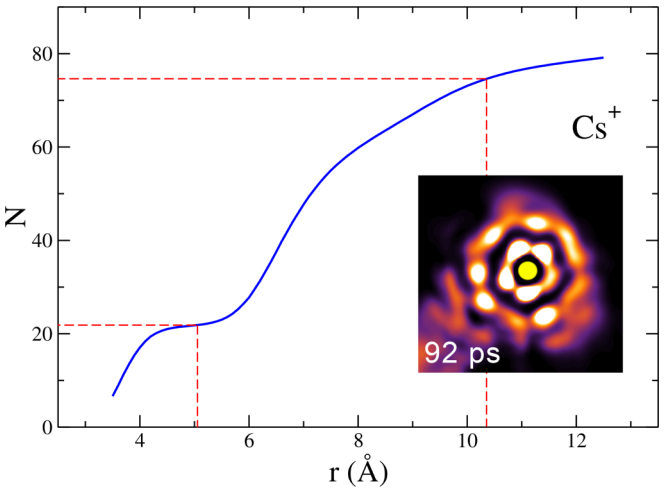

FIG. 8. (Color online) Helium atoms dynamically carried away around Cs^+ at $t = 92$ ps. The shorter horizontal dashed line indicates the number of He atoms in the first solvation shell, and the other line indicates the the total number of He atoms in the ejected, charged nanocluster. The inset shows the appearing snowball from which the distance r is defined.

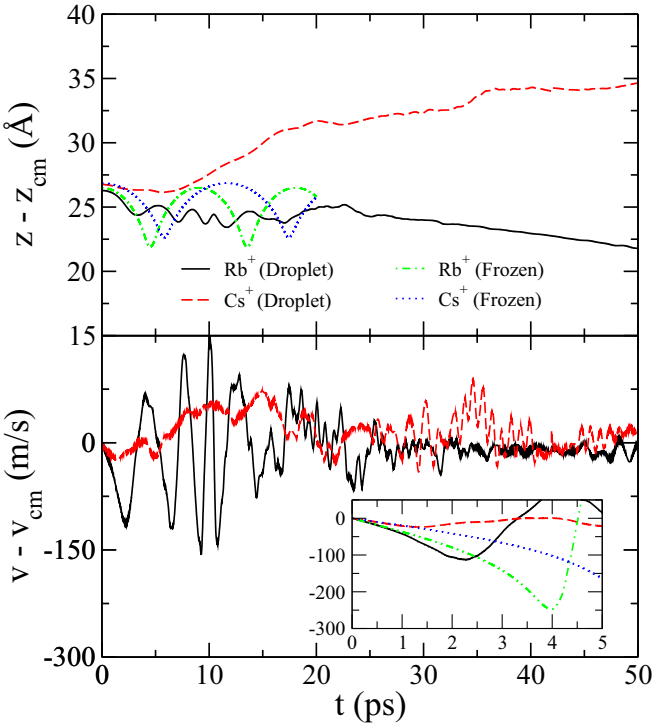

FIG. 9. (Color online) Position and speed of the alkali cation with respect to the helium center of mass as a function of time for the full calculations and for that carried out using the frozen helium density corresponding to the initial conditions. The inset shows the evolution during the first 5 ps.

the interaction strength of Rb^+ and Cs^+ with helium are very similar, the outcome is dramatically different.

We would like to stress that the conspicuous breaking of the axial symmetry in the case of Rb^+ and Cs^+ is not a numerical artifact but the result of the spontaneous symmetry breaking caused by the appearance of the highly structured snowball around the cation. Some details of the subsequent dynamic evolution might depend on the actual conditions of numerical procedure we have used to solve the TDDFT equations such as time and space steps, for instance, that have been chosen by a compromise between accuracy and computational feasibility. Although we cannot disregard that the appearance of these effects are eased by some unavoidable numerical inaccuracies when handling densities as those displayed in Figs. 1 and 2, the effect is rooted on a solid physical ground.

To gain insight into the solvation dynamics we have plotted in Fig. 9 the relative position and velocity of the cation with respect to the center of mass of the droplet. Inspection of this figure reveals that the outcome is already determined during the first few picoseconds of the dynamics. For both systems, the ion starts moving towards the center of the droplet upon its creation. In the case of Ba^+, the velocity of the ion was found to increase rather smoothly with time during the initial phase of the solvation [28]. This is quite different for Rb^+ and Cs^+; after their initial acceleration towards the droplet center, these ions are slowed down and start to move in the opposite direction (see also multimedia material corresponding to Figs. 6, 7, and 9). In the case of Rb^+, the ion reaches a maximum velocity of 112 m/s before it is slowed down and changes its direction after 3.3 ps. During this time the ion has traveled 1.9 Å and penetrated into the droplet. As time goes on the ion accelerates away from the droplet, slows down again, and eventually changes direction anew. This process repeats itself with a period of approximately 3 ps for about 25 ps after which the ion remains almost stationary and becomes solvated by the helium droplet. The Cs^+ ion performs a somewhat similar motion but with a very different outcome. At the start of the evolution the Cs^+ ion is accelerated towards the droplet center but only reaches a speed of 24 m/s before it slows down again. When it comes to a standstill after 3.3 ps it has moved only 0.42 Å and is still at the surface of the droplet. From 5.5 ps onwards the Cs^+ moves away from the droplet from which it eventually desorbs after $t \gtrsim 90$ ps.

As the outcome of the dynamics appears to be determined during the first few picoseconds it raises the question as to what is the origin for the different behavior during the initial phase. Obviously the initial position of the ion will affect the outcome. Upon creation the Ba^+ ion is located in a rather deep dimple while the alkali ions are located considerably further away from the droplet surface, as reflected by the distance between the ion and the helium droplet center of mass which amounts to 25.5, 26.5, and 26.9 Å for Ba^+, Rb^+, and Cs^+, respectively. Consequently, one expects that the Ba^+ ion becomes most easily solvated. The difference in the dynamics of Rb^+ and Cs^+ is not that easily accounted for. Analysis of the ions' motion reveals that the evolution of both systems during the first picosecond is determined by the cation-droplet interaction potential corresponding to the initial condition. This signifies that deformation of the droplet is not important up to this time. Calculations performed using a frozen helium distribution reveal that if the ions were to evolve according to the initial potential they would perform an oscillatory motion with a period of 9 and 11.5 ps for Rb^+ and Cs^+, respectively (see Fig. 9). The fact that a quite different motion is observed at longer times has to be attributed to a

change in the helium density. This change occurs after 1–2 ps as can be seen from the inset of Fig. 9, which compares the velocity of the ions found in the simulations and calculated using the frozen helium density approximation. Analysis of the helium densities suggests that the helium atoms located in the surface region close to the cation are involved. The light helium atoms are expected to be quickly accelerated towards the heavy cation due to the strong Ak^+-He interaction. The helium atoms rushing into the ion will slow it down, or even change its direction. Eventually these helium atoms will bind to the cation to form a snowball structure. At this point the interaction of the cation with the rest of the droplet becomes significantly weakened due to the screening of the ionic charge by the surrounding helium atoms. Depending on the velocity of the snowball and the strength of its interaction with the rest of the droplet it might or might not become solvated.

Thus, solvation, snowball formation, and desorption are dynamical processes that are not simply determined by the energy balance. They are affected by other properties as well, like the size of the helium droplet. As discussed above, the Cs^+ cation does not become solvated by a $^4He_{1000}$ droplet. As the ionic radius is fairly large compared to that of the helium droplet, curvature effects might contribute to a weakening of the ion-droplet effective interaction. Unfortunately, addressing the dynamics of doped droplets with a number of helium atoms significantly larger than $N = 1000$ is computationally very demanding. Preliminary results for $Cs^+@^4He_{2000}$ seem to indicate that in this case the Cs^+ cation becomes solvated by the helium. To establish the behavior for even larger systems we have carried out a series of simulations in which an impurity on a planar helium surface is suddenly ionized. This system has no curvature limitations, and locally mimics a very large droplet. To prevent the spurious bouncing back of the density waves at the walls of the simulation cell an absorbing potential has been added at its boundaries [71]. Figure 10 shows snapshots of the simulation of a Cs atom on a planar helium surface that is suddenly ionized [70]. At variance with the results for the $N = 1000$ droplet, the Cs^+ cation becomes solvated. This difference can be traced back to the initial phase of the evolution. In Fig. 11 the acceleration of the Cs ion during the initial phase of the evolution is plotted. The results for the droplet and the planar surface are very similar during the first few picoseconds, except that the magnitude of the acceleration is slightly larger for the planar surface. As a result, the ion travels further into helium before it is decelerated. This affects the later dynamics and eventually leads to the solvation of the ion. The small difference in the initial acceleration is directly related to the difference in the initial interaction potential. This in turn is fully determined by the helium density distribution resulting from the interaction of the neutral atom with the helium.

The dynamical processes found in this study are closely related to those occurring when ionizing pure helium droplets. As first observed by Gspann, electron impact ionization of He clusters leads to the formation of charged nanoclusters with sizes similar as found for Cs^+ [72]. In those experiments an impinging electron ionizes a helium atom. When this happens at the droplet surface, the situation is rather similar to that in our simulations. The explanation proposed by Gspann for the formation of what he called minicluster ions is essentially the one we have found in our simulations, i.e., the positive

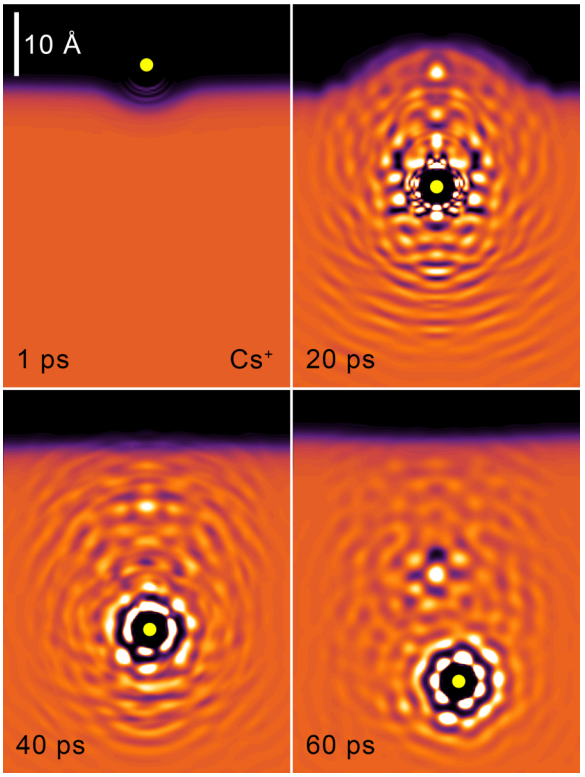

FIG. 10. (Color online) Dynamic evolution of the Cs^+ cation after sudden ionization of the neutral Cs atom sitting in a dimple on a planar helium surface. The corresponding time is indicated in each frame.

charge leads to the formation of a snowball due to the electrostrictive polarization of the surrounding helium. This charged nanocluster may be subsequently expelled from the parent droplet helped by the energy acquired by the ion in the course of the snowball formation.

As indicated in the Introduction, the solvation of Ba^+ is accompanied by the nucleation of a quantized ring vortex.

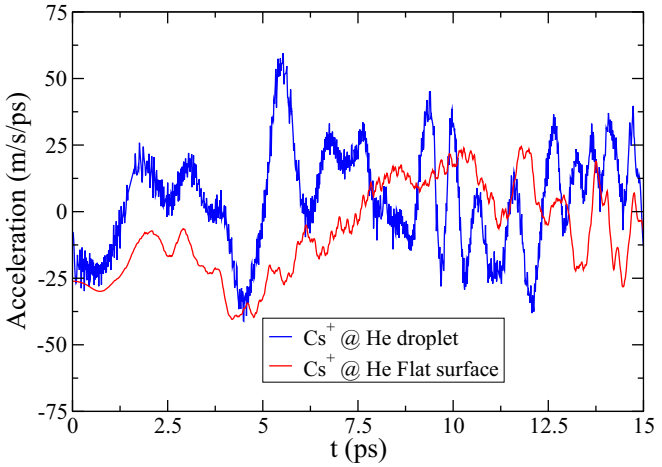

FIG. 11. (Color online) Acceleration experienced by a Cs^+ cation during the initial phase of the solvation after its creation on a $N = 1000$ helium droplet and a flat helium surface.

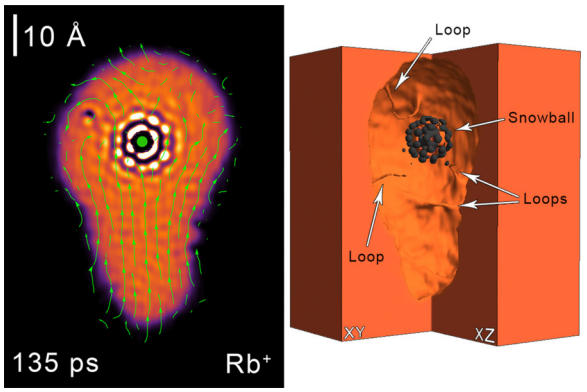

FIG. 12. (Color online) Right: Three-dimensional view of the Rb^+-droplet complex at $t = 135$ ps showing the appearance of several vortex loops attached to the droplet surface and the snowball around the cation. Left: The corresponding circulation lines on the x-z plane cutting a vortex loop.

The same is expected for the solvation of the Rb^+ and Cs^+ cations. In our work on barium we have shown that the speed of the cation has to exceed the critical Landau velocity for a few picoseconds so that the vortex ring has time to nucleate [28]. This condition is not fulfilled in the present simulations, neither for Rb^+ nor for Cs^+ (see Fig. 9). This is most likely related to the same processes leading to the desorption of the Cs^+. During the initial phase of the dynamics when the ion moves towards the droplets it is quickly slowed down by the nearby helium atoms rushing in to form a snowball. Once the snowball has formed the cation-droplet interaction is efficiently screened, thereby limiting the maximum achievable velocity.

Interestingly, we find that in spite of the low velocity of the Rb^+, vortices are nucleated. These result from the large distortions of the droplet surface caused by the solvation of Rb^+ which acts as nucleation seeds. In contrast to the results of our previous work, no vortex rings are formed but quantized vortex loops whose ends are both attached to the droplet surface [73,74]. One such configuration is displayed in Fig. 12 [70]. The rather distorted vortex loops found here bear some geometric similarity to the equilibrium configurations of the curved vortices described in Refs. [22,75]. While these simulations do not reveal the nucleation of vortex rings this does not imply that these cannot form. As a matter of fact, the simulation using the Koutselos Rb^+-He pair potentials reveals the nucleation of a quantized vortex ring induced by the droplet deformation. This signifies that vortex nucleation by droplet deformations is a very common process and that the exact shape of these vortices is determined by the finer details of the system. Finally, we mention that we have not seen any ring vortex nucleated in the helium free surface geometry for any of the cations of this study. Most likely, this is related to the very different surface distortions and density waves propagating through the free surface as compared to a droplet.

IV. SUMMARY

We have investigated by means of TDDFT the solvation dynamics of Rb^+ and Cs^+ formed at the surface of He_{1000} droplets. The solvation dynamics initially proceeds by the motion of the cation towards the droplet center due to the attractive interaction between the cation and the helium. Due to the large interaction strength, helium atoms in the surface region are quickly accelerated towards the ion forming a so-called snowball, i.e., a solidlike helium solvation structure. In the case of Rb^+ this process is complete after 10 ps. At longer times the snowball becomes solvated by the helium droplet which rearranges itself around the stationary ion. The large density fluctuations induced by the Rb^+ solvation process lead to the nucleation of quantized vortices. Depending on the details of the system, these can be either loop or ring vortices. In the case of Cs^+, the initial phase of the snowball formation prevents the ion from penetrating the helium droplet. The snowball therefore forms at the surface of the droplet in about 30 ps. Due to the effective shielding of the Cs^+ charge by its surrounding helium atom, it is only very weakly bound to the droplet. As a result, the Cs^+ snowball desorbs after 90 ps from the droplet due to helium density fluctuations.

The simulations reveal that the final outcome of the dynamics is strongly determined by the initial phase of the evolution. In the case of the alkalis investigated here, the snowball formation initiated by the strong interaction of the cation with helium hinders a direct solvation of the ion as was observed for Ba^+ which has a much weaker interaction with the helium [28]. The initial phase of the solvation process depends not only critically on the interaction strength between the ion and the helium, but also on the initial helium configuration. In particular, there is a clear droplet-size dependence especially apparent in the case of Cs, as simulations of Cs^+ on a flat helium surface have revealed. This reconciles the outcome of our calculations, carried out for a fairly small droplet, with the well established experimental fact that upon *in situ* ionization of the neutral species, Ba, Rb, and Cs cations remain attached to helium droplets made of several thousand atoms [29–32]. It should be noted, however, that in these experiments the alkalis have been ionized via an intermediate state.

Concluding, the solvation of surface located ions in helium droplets is not solely determined by the energy balance but depends strongly on the finer details of the system under study. As a result, the outcome can be very different for what appear to be very similar systems.

ACKNOWLEDGMENTS

We would like to thank Massimo Mella and Frank Stienkemeier for useful discussions. This work has been performed under Grant No. FIS2011-28617-C02-01 from DGI, Spain (FEDER), Grant No. 2014SGR401 from Generalitat de Catalunya, and Grant No. 200021-146598 from the Swiss National Science Foundation. A.L. has been supported by the ME (Spain) FPI program, Grant No. BES-2012-057439.

[1] B. Tabbert, H. Günter, and G. zu Putlitz, J. Low Temp. Phys. **109**, 653 (1997).

[2] M. Foerste, H. Guenther, O. Riediger, J. Wiebe, and G. zu Putliz, Z. Phys. B: Condens. Matter **104**, 317 (1997).

[3] M. Rossi, M. Verona, D. E. Galli, and L. Reatto, Phys. Rev. B **69**, 212510 (2004).
[4] S. L. Fiedler, D. Mateo, T. Aleksanyan, and J. Eloranta, Phys. Rev. B **86**, 144522 (2012).
[5] K. R. Atkins, Phys. Rev. **116**, 1339 (1959).
[6] M. Hartmann, R. E. Miller, J. P. Toennies, and A. Vilesov, Phys. Rev. Lett. **75**, 1566 (1995).
[7] D. M. Brink and S. Stringari, Z. Phys. D **15**, 257 (1990).
[8] P. Sindzingre, M. L. Klein, and D. M. Ceperley, Phys. Rev. Lett. **63**, 1601 (1989).
[9] M. V. Rama Krishna and K. B. Whaley, Phys. Rev. Lett. **64**, 1126 (1990).
[10] S. A. Chin and E. Krotscheck, Phys. Rev. B **45**, 852 (1992).
[11] E. Krotscheck and R. Zillich, J. Chem. Phys. **115**, 10161 (2001).
[12] S. Grebenev, J. P. Toennies, and A. Vilesov, Science **279**, 2083 (1998).
[13] N. B. Brauer, S. Smolarek, E. Loginov, D. Mateo, A. Hernando, M. Pi, M. Barranco, W. J. Buma, and M. Drabbels, Phys. Rev. Lett. **111**, 153002 (2013).
[14] D. Mateo, A. Hernando, M. Barranco, E. Loginov, M. Drabbels, and M. Pi, Phys. Chem. Chem. Phys. **15**, 18388 (2013).
[15] L. F. Gomez, E. Loginov, and A. F. Vilesov, Phys. Rev. Lett. **108**, 155302 (2012).
[16] D. Spence, E. Latimer, C. Feng, A. Boatwright, A. M. Ellis, and S. Yang, Phys. Chem. Chem. Phys. **16**, 6903 (2014).
[17] E. Latimer, D. Spence, C. Feng, A. Boatwright, A. M. Ellis, and S. Yang, Nano Lett. **14**, 2902 (2014).
[18] Ph. Thaler, A. Volk, F. Lackner, J. Steurer, D. Knez, W. Grogger, F. Hofer, and W. E. Ernst, Phys. Rev. B **90**, 155442 (2014).
[19] L. F. Gomez *et al.*, Science **345**, 906 (2014).
[20] J. P. Toennies and A. F. Vilesov, Angew. Chem., Int. Ed. **43**, 2622 (2004).
[21] F. Dalfovo, R. Mayol, M. Pi, and M. Barranco, Phys. Rev. Lett. **85**, 1028 (2000).
[22] K. K. Lehmann and R. Schmied, Phys. Rev. B **68**, 224520 (2003).
[23] F. Stienkemeier and K. K. Lehmann, J. Phys. B **39**, R127 (2006).
[24] M. Y. Choi, G. E. Douberly, T. M. Falconer, W. K. Lewis, C. M. Lindsay, J. M. Merritt, P. L. Stiles, and R. E. Miller, Int. Rev. Phys. Chem. **25**, 15 (2006).
[25] J. D. Close, F. Federmann, K. Hoffmann, and N. Quaas, J. Low Temp. Phys. **111**, 661 (1998).
[26] F. Ancilotto, M. Barranco, and M. Pi, Phys. Rev. Lett. **91**, 105302 (2003).
[27] A. Hernando, M. Barranco, R. Mayol, M. Pi, and M. Krosnicki, Phys. Rev. B **77**, 024513 (2008).
[28] D. Mateo, A. Leal, A. Hernando, M. Barranco, M. Pi, F. Cargnoni, M. Mella, X. Zhang, and M. Drabbels, J. Chem. Phys. **140**, 131101 (2014).
[29] M. Theisen, F. Lackner, and W. E. Ernst, Phys. Chem. Chem. Phys. **12**, 14861 (2010).
[30] E. Loginov and M. Drabbels, Phys. Rev. Lett. **106**, 083401 (2011).
[31] M. Theisen, F. Lackner, G. Krois, and W. E. Ernst, J. Phys. Chem. Lett. **2**, 2778 (2011).
[32] M. Theisen, F. Lackner, and W. E. Ernst, J. Chem. Phys. **135**, 074306 (2011).
[33] X. Zhang and M. Drabbels, J. Chem. Phys. **137**, 051102 (2012).
[34] S. Müller, M. Mudrich, and F. Stienkemeier, J. Chem. Phys. **131**, 044319 (2009).
[35] S. H. Patil, J. Chem. Phys. **94**, 8089 (1991).
[36] T. V. Tscherbul, P. Zhang, H. R. Sadeghpour, and A. Dalgarno, Phys. Rev. A **79**, 062707 (2009).
[37] G. Guillon, A. Viel, and J.-M. Launay, J. Chem. Phys. **136**, 174307 (2012).
[38] A. Ponti and F. Cargnoni (unpublished).
[39] A. D. Koutselos, E. A. Mason, and L. A. Viehland, J. Chem. Phys. **93**, 7125 (1990).
[40] H.-J. Werner *et al.*, *MOLPRO, version 2010.1, a package of ab initio programs*, see http://www.molpro.net.
[41] I. S. Lim, P. Schwerdtfeger, B. Metz, and H. Stoll, J. Chem. Phys. **122**, 104103 (2005).
[42] F. Weigend and R. Ahlrichs, Phys. Chem. Chem. Phys. **7**, 3297 (2005).
[43] D. E. Woon and T. H. Dunning, Jr., J. Chem. Phys. **100**, 2975 (1994).
[44] F.-M. Tao, Z. Li, and Y.-K. Pan, Chem. Phys. Lett. **255**, 179 (1996).
[45] S. F. Boys and S. Bernardi, Mol. Phys. **19**, 553 (1970).
[46] T. Leininger, A. Nicklass, W. Kuekhle, H. Stoll, M. Dolg, and A. Bergner, Chem. Phys. Lett. **255**, 274 (1996).
[47] F. Dalfovo, A. Lastri, L. Pricaupenko, S. Stringari, and J. Treiner, Phys. Rev. B **52**, 1193 (1995).
[48] M. Barranco, R. Guardiola, S. Hernández, R. Mayol, J. Navarro, and M. Pi, J. Low Temp. Phys. **142**, 1 (2006).
[49] L. Giacomazzi, F. Toigo, and F. Ancilotto, Phys. Rev. B **67**, 104501 (2003).
[50] L. Lehtovaara, T. Kiljunen, and J. Eloranta, J. Comput. Phys. **194**, 78 (2004).
[51] A. Hernando, M. Barranco, M. Pi, E. Loginov, M. Langlet, and M. Drabbels, Phys. Chem. Chem. Phys. **14**, 3996 (2012).
[52] F. O. Ellison, J. Am. Chem. Soc. **85**, 3540 (1963).
[53] F. Ancilotto, E. Cheng, M. W. Cole, and F. Toigo, Z. Phys. D **98**, 323 (1995).
[54] F. Ancilotto, M. Barranco, F. Caupin, R. Mayol, and M. Pi, Phys. Rev. B **72**, 214522 (2005).
[55] F. Ancilotto, M. Pi, R. Mayol, M. Barranco, and K. K. Lehmann, J. Phys. Chem. A **111**, 12695 (2007).
[56] O. Bünermann, G. Droppelmann, A. Hernando, R. Mayol, and F. Stienkemeier, J. Phys. Chem. A **111**, 12684 (2007).
[57] M. Frigo and S. G. Johnson, Proc. IEEE **93**, 216 (2005).
[58] A. Ralston and H. S. Wilf, *Mathematical Methods for Digital Computers* (Wiley, New York, 1960).
[59] F. Stienkemeier, J. Higgins, C. Callegari, S. I. Kanorsky, W. E. Ernst, and G. Scoles, Z. Phys. D **38**, 253 (1996).
[60] D. E. Galli, D. M. Ceperley, and L. Reatto, J. Phys. Chem. A **115**, 7300 (2011).
[61] S. Paolini, F. Ancilotto, and F. Toigo, J. Chem. Phys. **126**, 124317 (2007).
[62] E. Loginov and M. Drabbels, J. Chem. Phys. **136**, 154302 (2012).
[63] D. Mateo, A. Hernando, M. Barranco, R. Mayol, and M. Pi, Phys. Rev. B **83**, 174505 (2011).
[64] C. C. Lovallo and M. Klobukowski, J. Chem. Phys. **120**, 246 (2004).

[65] A. Kramida, Y. Ralchenko, J. Reader, and NIST ASD Team (2012), NIST Atomic Spectra Database (version 5.0), National Institute of Standards and Technology, Gaithersburg, MD, http://physics.nist.gov/asd.

[66] E. Loginov, D. Rossi, and M. Drabbels, Phys. Rev. Lett. **95**, 163401 (2005).

[67] F. Lackner, G. Krois, M. Theisen, M. Koch, and W. E. Ernst, Phys. Chem. Chem. Phys. **13**, 18781 (2011).

[68] F. Lackner, G. Krois, M. Koch, and W. E. Ernst, J. Phys. Chem. Lett. **3**, 1404 (2012).

[69] E. Loginov and M. Drabbels, J. Phys. Chem. A **118**, 2738 (2014).

[70] See Supplemental Material at http://link.aps.org/supplemental/10.1103/PhysRevB.90.224518 for the continuous movie corresponding to Figs. 6, 7, and 10.

[71] D. Mateo, D. Jin, M. Barranco, and M. Pi, J. Chem. Phys. **134**, 044507 (2011).

[72] J. Gspann, Surf. Sci. **106**, 219 (1981).

[73] C. M. Muirhead, W. F. Vinen, and R. J. Donnelly, Philos. Trans. R. Soc. London, Ser. A **311**, 433 (1984).

[74] R. J. Donnelly, *Quantized Vortices in Helium II*, Cambridge Studies in Low Temperature Physics Vol. 3 (Cambridge University Press, Cambridge, UK, 1991).

[75] G. H. Bauer, R. J. Donnelly, and W. F. Vinen, J. Low Temp. Phys. **98**, 47 (1995).